Available online at www.sciencedirect.com
SCIENCE DIRECT®
ELSEVIER
Palaeogeography, Palaeoclimatology, Palaeoecology 207 (2004) 105–125
PALAEO
www.elsevier.com/locate/palaeo

Periodic components in the diversity of calcareous plankton and geological events over the past 230 Myr☆

Andreas Prokoph[a,*], Michael R. Rampino[b,c,1], Hafida El Bilali[d,2]

[a] SPEEDSTAT, 36 Corley Private, Ottawa, ON, Canada K1V 8T7
[b] Earth and Environmental Sciences Program, New York University, 100 Washington Square East, New York, NY 10003, USA
[c] NASA, Goddard Institute for Space Studies, 2880 Broadway, New York, NY 10025, USA
[d] Ottawa-Carleton Geoscience Centre and Department of Earth Sciences, University of Ottawa, 140 Louis Pasteur, Ottawa, ON, Canada K1N 6N5

Received 22 July 2003; received in revised form 16 January 2004; accepted 6 February 2004

Abstract

We performed statistical analysis on high-resolution records of the diversity of calcareous plankton (planktonic foraminifera and calcareous nannoplankton), and on records of global sea level, marine isotopes ($\delta^{18}O$, $\delta^{13}C$, $^{87}Sr/^{86}Sr$), large igneous province (LIP) eruptions, and dated impact craters over the last 230 Myr. Results of Continuous Wavelet Analysis (CWT), Fast Fourier Transform (FFT) spectral analysis and cross-spectral analysis indicate that the records of diversity of calcareous nannoplankton (CN) and planktonic foraminifera (PF) and all of the geologic time series tested show similar dominant 25–33 Myr cycles. Based on the statistical results, best-fit stationary-periodic models for PF and CN evolutionary records can be constructed (with t = time in Myr): CN diversity = $9.5 \sin(2\pi(t - 7.5 \text{ Myr})/29 \text{ Myr}) + 4.8 \sin(2\pi(t - 4 \text{ Myr})/15.3 \text{ Myr})$, and PF diversity = $7.6 \sin(2\pi(t - 12 \text{ Myr})/26 \text{ Myr}) + 3 \sin(2\pi t/9.2 \text{ Myr})$.

These periodic models describe major patterns in the diversity history, such as: (1) a sawtooth-shaped 29-Myr cycle for calcareous nannoplankton diversity, with gradual increases and abrupt decreases in diversity; (2) plateau-shaped ~26-Myr cycles in the planktonic foraminiferal record, with abrupt diversity increases and decreases; and (3) the presence of ~15.3- and 9.2-Myr periodic components that modify the shapes of the 26- to 29-Myr cycles.

Except for the synchronous decreases in diversity of PF and CN at 65 and ~34 Ma, the diversity extrema for the two planktonic groups have been on average ~2 to 3 Myr out of phase. In the ~30-Myr-cycle band, CN diversity increased with sea-level rise and increased paleotemperatures, whereas PF diversity was, in general, greater during times of lower sea levels. Diversity of PF and CN was reduced at times of major LIP eruptions and large impacts that follow ~15 or 30 Myr periodicities. These results suggest that the diversity of calcareous plankton since their appearance in the early Mesozoic has been modulated by long-term cyclical changes in global environmental conditions and by periodic large volcanic and impact events. The pacemaker, or pacemakers, for these cycles may be astrophysical, geophysical or some combination of the two.

Keywords: Planktonic foraminifera; Calcareous nannoplankton; Diversity; Evolution; Cycles; Time-series analysis

☆ Supplementary data associated with this article can be found, in the online version, at doi: 10.1016/ j.palaeo.2004.02.004.

* Corresponding author. Fax: +1-613-562-5192.
E-mail addresses: aprokocon@aol.com (A. Prokoph), mrr1@nyu.edu (M.R. Rampino), helbilal@aix1.uottawa.ca (H. El Bilali).
[1] Fax: +1-212-995-4015.
[2] Fax: +1-613-562-5192.

0031-0182/$ - see front matter © 2004 Elsevier B.V. All rights reserved.
doi:10.1016/j.palaeo.2004.02.004

1. Introduction

The first step in the development of a theory of causation is the recognition of patterns. Statistical analysis has proven to be a useful tool in detecting patterns in the time history of geologic and biotic events, thus providing clues to the possible causes of the variations in biological diversity that mark Earth history (e.g., Raup and Sepkoski, 1986; Rampino and Caldeira, 1993; Liritzis, 1993; Prokoph et al., 2000). Such statistical studies are dependent on: (1) The accuracy, precision, resolution and comparability of the time scales used for the correlation of biostratigraphic data with other kinds of geologic records, (2) the completeness of the records, and (3) the accuracy and precision of measures of the amplitudes of the various records. For example, Rampino and Caldeira (1993) searched the geological literature, compiled records of geologic and biotic events and applied statistical analysis in order to search for possible periodicities and correlations among these time series. Over the last decade, there have been significant improvements in the geological time scale (Gradstein and Ogg, 1996; Okulitch, 2002); the record of biotic diversity for a number of groups (e.g., Prokoph et al., 2000); the precision, accuracy, and completeness of records of large-scale igneous activity (e.g., Ernst and Buchan, 2001; Courtillot and Renne, 2003), impact cratering (e.g., Grieve, 1997 and recent updates); sea-level history (e.g., Hardenbol et al., 1998); and long-term isotopic records of the marine environment and climate (e.g., Veizer et al., 1999; Zachos et al., 2001).

In this paper, we quantitatively examine high-resolution records of diversity of two widespread, important marine groups—planktonic foraminifera (PF) and calcareous nannoplankton (CN). These planktonic groups with calcareous skeletons have inhabited the ocean since the Jurassic and Late Triassic, respectively, and are good indicators of physical–chemical conditions (e.g., temperature, salinity, oxygenation), nutrient availability, and the stratification and stability of marine surface waters. In order to search for possible common periodicities and correlations among the records of plankton diversity, major geologic events and long-term environmental trends, we applied several types of time-series analysis and cross-correlation analysis to these compilations of evolutionary and geologic data.

2. Data and methods

2.1. Time scales and age-uncertainties

Geological time scales are subject to age uncertainties due to inaccuracies and limited precision in: (1) decay constants of radiogenic elements, (2) the radiogenic age of a mineral compared to its time of crystallization (e.g., 'reservoir effects'), and (3) the definition and absolute dating of biostratigraphic units and their boundaries (Remane, 2003). At present, the precision of dates for geological events and stratigraphic boundaries is commonly high, but U/Pb ages are consistently $2\sigma = \sim 2\%$ different (mostly older) than comparable Ar/Ar ages, and the U/Pb ages are considered more reliable (Mundil et al., 2001). Because the recently published time scale of Okulitch (2002) incorporates many single-grain U/Pb zircon dates for the Jurassic and Triassic Periods (Palfy et al., 2000a,b), we used this time scale in our analysis. To provide a statistically robust database, the biostratigraphically controlled geological and fossil records have been transferred to the Okulitch (2002) time scale by linear interpolation between stage and/or zone boundaries. Because of uncertainties in the time scale, biostratigraphy, and geochronology of geological events, we performed statistical analysis for the various records at 1-Myr intervals.

2.2. Evolutionary records of calcareous plankton

Planktonic foraminifera (PF) and calcareous nannoplankton (CN) are useful for long-term studies of biotic diversity because they are globally distributed in Mesozoic and Cenozoic marine deposits (Hart, 1990; Prokoph et al., 2000; Bown et al., 1992), and extensive, well-established high-resolution databases now exist (Bown et al., 1992 and update; Prokoph et al., 2000; Patterson et al., in press). CN combines all calcareous phytoplanktonic organisms (mostly coccoliths, a family of calcareous algae, and nannoconids).

The record of planktonic foraminiferal diversity utilized for time-series analysis (Patterson et al., in

press) is composed of the stratigraphic ranges of 518 species at 206 stratigraphic stages from the present back to the Early Jurassic (Fig. 1). Here, we applied time-series analysis on PF diversity data for 193 stratigraphic stages for the last 121.5 Ma (back to the Barremian/Aptian Boundary). Preliminary analyses indicated that the earlier Cretaceous and Jurassic record is not robust enough for statistical analysis, especially as there is ongoing debate as to which of the older foraminifera were planktonic versus benthic (R.T. Patterson, R.M. Leckie, personal communication).

The fossil record of calcareous nannoplankton (Bown et al., 1992) contains numbers of species from 105 stages in the last 227 Myr. Here, we used an updated record (Bown, personal communication) of CN (and separate coccolith diversity) for 75 stages. As there is still controversy as to whether many PF and CN morphotypes are different species (genotypes) or rather phenotypes of the same species, we analyzed only the diversity records of PF and CN and not the speciation/extinction and turnover records.

For the purpose of evaluation of the long-term evolutionary behavior of calcareous nannoplankton and planktonic foraminifera, we constructed time series for the relative changes in diversity of PF and CN per Myr (Fig. 1). We also constructed binary time

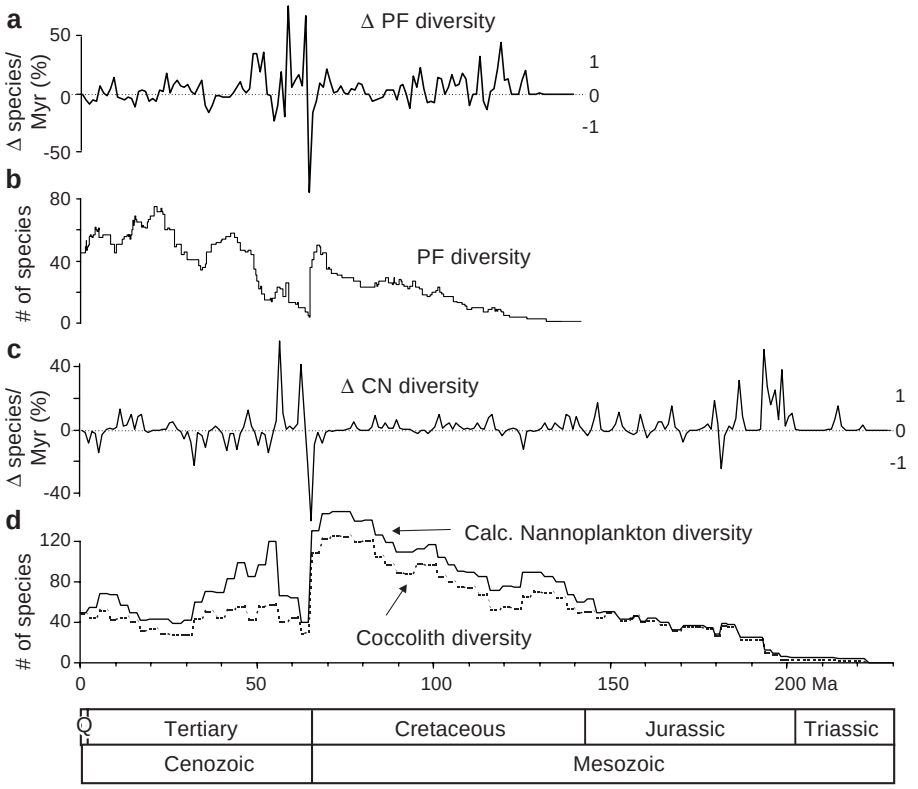

Fig. 1. Comparison of diversity of calcareous nannoplankton, coccoliths (Bown et al., 1992; Bown, personal communication), and planktonic foraminifera (Patterson et al., in press). (a) Relative planktonic foraminiferal (PF) diversity changes per 1 Myr (in %). Horizontal dotted line marks no changes (0 in binary record, right side of graphic), above 0 indicates increasing diversity (1 in binary record), below 0 marks decreasing diversity (− 1 in binary record). (b) Planktonic foraminiferal (PF) diversity record (Patterson et al., in press) for 198 zones over the last 142 Ma. (c) Relative calcareous nannofossil (CN) diversity changes per 1 Myr (in %). Horizontal dotted line marks no changes (0 in binary records, right side of graphic), above 0 indicates increasing diversity (1 in binary record), below 0 marks decreasing diversity (− 1 in binary record). (d) CN (solid line) and coccolith (dashed line) diversity records (Bown et al., 1992; Bown, personal communication) for 75 zones over the last 222 Ma. (Time scale after Okulitch, 2002; Q indicates Quaternary.)

series of the relative changes in PF and CN diversity per Myr, with 1 = representing increased diversity, 0 = no change in diversity and −1 = decreasing diversity (Fig. 1). In this way, possible artificial cycles that may result from a few very high signals (e.g., the extinctions at the Cretaceous/Tertiary (K/T) boundary) can be suppressed.

2.3. Records of geological events

Geological events such as large impacts or episodes of volcanism are discretely distributed in time, which restricts the use of some statistical analysis methods for comparison with more continuous geological records (e.g., paleotemperatures, biological diversity). For this reason, the event records that we compiled were transformed into continuous time series at Myr time intervals through the use of Gaussian filtering, with each event assigned a value of 1 and a standard deviation according to its age uncertainty (e.g., Rampino and Caldeira, 1993).

The impact crater database was compiled from the most recent update of the terrestrial impact cratering list (Grieve, 1997, with updates). We included in our analysis 45 impact craters >5 km in diameter with defined age-uncertainties (Fig. 2e). Furthermore, a subset of 27 large impact craters ≥20 km diameter with 2σ age uncertainties of <32 Myr (92% with errors < 10 Myr) was also examined. Based on the estimates of Chapman and Morrison (1989), the impact energy (J) in Mt TNT was calculated for the database by $J = 4.2d^{3.477}$, with d = crater diameter in km (Fig. 2e).

We also compiled ages and volumes of 31 Large Igneous Province (LIP) events with 2σ age uncertainties of <15 Myr (95% < 10 Myr, 40% < 2 Myr) from Ernst and Buchan (2001) and Courtillot and Renne (2003). The data were transformed into a continuous time series at a 1-Myr interval using Gaussian filtering. We separated a subset of 19 oceanic LIP events for tests of the possible influence of oceanic LIPs versus LIP events in general. We used the initiation age for each major LIP episode, as most of the volume of LIP events were erupted in the first million years (e.g., Rampino and Stothers, 1988; Ernst and Buchan, 2001; Courtillot and Renne, 2003). Furthermore, a separate time series of the volumes of LIP events was constructed (Fig. 2c) by multiplying the Gaussian age probability by the volume for each event. We consider the LIP record complete, because LIP volcanics are mostly easy detectable, thick and widespread. The time interval studied also postdates the opening of the Atlantic. The LIP volumes are uncertain because of extensive erosion and burial by younger deposits.

We also included in our compilation the occurrence times of 10 major oceanic anoxic events (Rampino and Caldeira, 1993; Leckie et al., 2002), and the times of 10 mass extinction events (Raup and Sepkoski, 1986) in the last 230 Myr (Fig. 2d). We use these data for graphic correlation only, however, as their relatively low number does not support robust statistical analysis.

2.4. Sea-level fluctuations and marine isotope records

Changes in global sea level reconstructed from seismic data (Fig. 2b) (Hardenbol et al., 1998), and the record of variations in the isotopic ($^{87}Sr/^{86}Sr$, $\delta^{13}C$ and $\delta^{18}O$) composition of seawater are proxies for continuous environmental changes over geologic time. For our isotope data base, we used 2399 $^{87}Sr/^{86}Sr$ data points (Veizer et al., 1999; Bralower et al., 1997), 1948 $\delta^{13}C$ data points, and 2013 $\delta^{18}O$ data points (Veizer et al., 1999; Voigt, 2000; Leckie et al., 2002) that were extracted from low-Mg calcite shells and tests of brachiopods, belemnites, oysters, planktonic and benthic foraminifera of low and mid latitude sites. The isotope data are stratigraphically unevenly distributed. All isotope records have gaps in the Norian (Late Triassic). Several long gaps in the $\delta^{13}C$ and $\delta^{18}O$ record exist also in Callovian/Bathonian (~ 3 Myr gap), Late Aptian (~ 5 Myr gap), Cenomanian (~ 7 Myr gap), Coniacian–Early Campanian (~ 11 Myr gap) and Late Campanian (4 Myr gap). Jurassic to recent data are predominantly from the subtropics and mid-latitudes. The Triassic data are from the tropical realm (Veizer et al., 1999). The isotope data have been transformed into continuous time series using age uncertainties of $2\sigma = \pm 1\%$ (Fig. 2a,b) that reflect the inaccuracy of the timescale (Agterberg, 1994) and biostratigraphic uncertainties.

2.5. Statistical methods

In our time-series analyses, we utilized several methods including the Continuous Wavelet Trans-

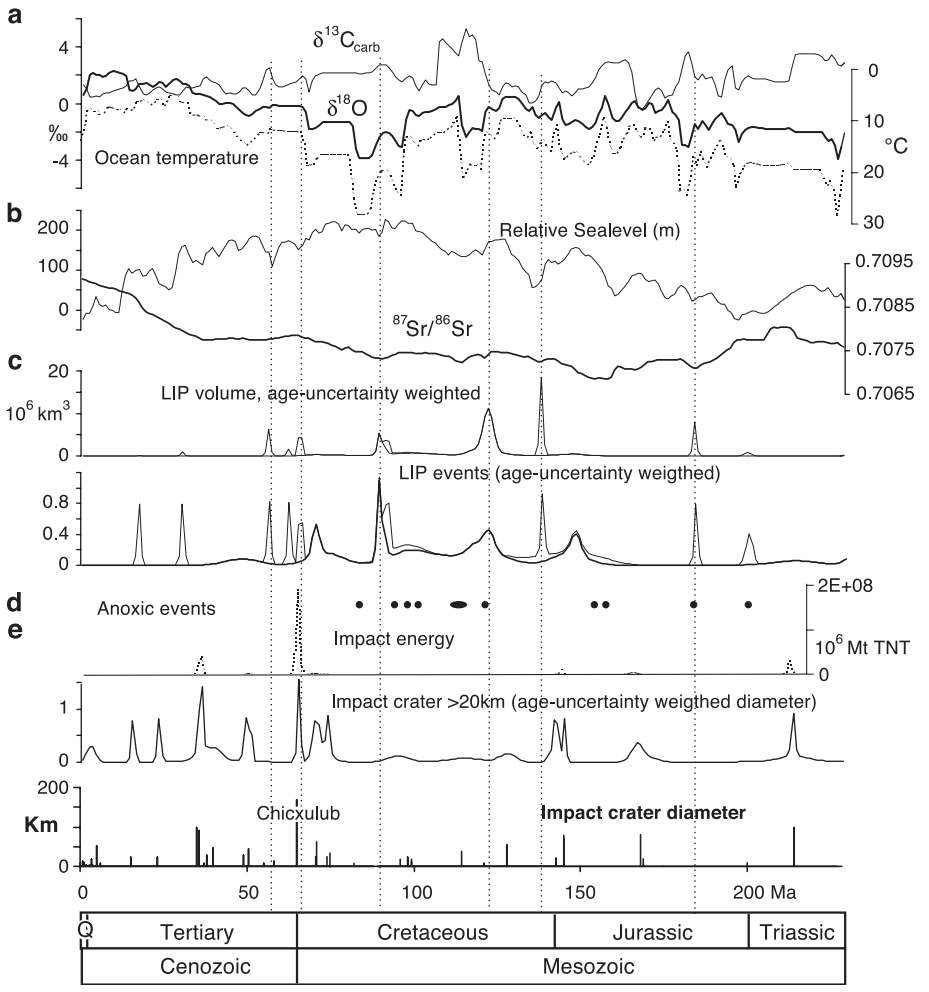

Fig. 2. Comparison of (a) $\delta^{13}C$ (solid line), $\delta^{18}O$ (bold solid line) of marine carbonates, in ‰ versus PDB (Veizer et al., 1999; with additional data from Leckie et al., 2002; Voigt, 2000), and ocean temperature (dashed line) calculated from $\delta^{18}O$ carbonate record according to Sellwood et al. (1994). (b) Relative sea-level changes in meters (Hardenbol et al., 1998); strontium isotopes of marine carbonates (Veizer et al., 1999; with additional data from Bralower et al., 1997). (c) Records of all (solid lines) and oceanic (bold solid lines) Large Igneous Province (LIP) eruptions (Ernst and Buchan, 2001; Courtillot and Renne, 2003). Upper: LIP volumes weighted by age uncertainties; lower: sum probability of occurrences in 1-Myr intervals. (d) Anoxic events (Rampino and Caldeira, 1993; Kerr, 1998; Leckie et al., 2002) at 84.5, 93.5, 99, 102, 109–112, 120.5, 155, 157, 184 and 200 Myr ago. (e) Impact crater record (Grieve, 1997, and updates; Rampino, 2002). Top: impact energy estimated from crater diameter (for equation, see text); middle: impact crater diameter weighted (Gaussian filtering) by age uncertainties; lower: impact crater diameters at mean age estimates. Time scale after Okulitch (2002); vertical dashed lines for correlation between large LIP eruptions and other geological records.

form (CWT) method (Rioul and Vetterli, 1991), spectral analysis (Fast Fourier Transform), and cross-spectral analysis (e.g., Davis, 1986). Each of these methods has advantages and limits in the way they present signals in frequency (e.g., cycle length) domain, including bandwidth uncertainties, edge effects, and harmonics (frequency doubling effects). Continuous Wavelet Transform analysis has advantages over Fourier analysis in that each wavelet coefficient of a period or amplitude of a cycle can be related to a specific time interval (or location). The minimum wavelength is determined by the Nyquist

frequency, which is twice the average sampling interval.

We restricted our analysis to cycles and trends >6 Myr for the CN data, and to >5 Myr for all other records because of uncertainties in the time scale and in comparing geologic events dated by various methods. Higher-resolution analysis may be feasible for records restricted to the Cenozoic Era.

CWT produces a space of wavelet coefficients $W_\psi(a, b)$, of scale (e.g., wavelength) a and time b:

$$W_\psi(a,b) = \left(\frac{1}{a}\right)\int f(t)\psi\left(\frac{t-b}{a}\right)\mathrm{d}t \quad (1)$$

We used the Morlet wavelet (Grossman and Morlet, 1984):

$$\psi^1_{a,b}(t) = \pi^{-\frac{1}{4}}(al)^{-\frac{1}{2}}\mathrm{e}^{-i2\pi\frac{1}{a}(t-b)}\mathrm{e}^{-\frac{1}{2}\left(\frac{t-b}{al}\right)^2} \quad (2)$$

with l representative of the scaling ratio of the analysis window, which is set to $l=10$ providing particularly good resolution for paleoclimate and fossil records (e.g., Bolton et al., 1995; Appenzeller et al., 1998; Prokoph et al., 2000; Rampino et al., 2000). Data were standardized to a mean = 0, and a fitted trend line was removed. The graphic representation in the time–frequency space is a ''scalogram''. The bandwidth uncertainty df/f of the wavelet analysis is 0.0707 (~ 7%) for all wavelengths for the Morlet wavelet and $l=10$ as used here.

The wavelet coefficients at the beginning and end of a data set have an 'edge effect', because only one half of the Morlet wavelet lies inside the line-scan data set, and the missing data in the analysis windows are replaced ('padded') by zeros. The missing data can equal up to 50% of the analysis window, leading to a 50% decreased significance for the wavelet coefficient at bottom and top of a time series. This effect can result in artificially decreased or less commonly increased wavelet coefficients for a completely stationary periodic signal with constant amplitude. The edge effect decreases to zero towards the middle of the time series and for shorter wavelengths, and the boundary of edge effects on the wavelet coefficients forms a wavelength-dependent curve, called the 'cone of influence' (Torrence and Compo, 1998). The cones of influences for 95% significance, based the wavelet-analysis parameters used, are illustrated in the scalograms.

The series of wavelengths $a_{\mathrm{wmax}_{1\ldots3}}(b)$ with the three strongest local wavelet coefficient $W_{l(a,b)}$ has been extracted from the wavelet-coefficient matrix, because these series determine the locally strongest (i.e., most significant) cycle lengths, independent of their absolute amplitude compared to the rest of the time series analyzed.

We also applied spectral analysis using Fast Fourier Transform (FFT) on equidistant data sets. Because FFT requires equidistant data $x(t)$, it was necessary to interpolate all records to equal 1-Myr intervals. Fourier transform is defined by:

$$P_f^2 = \int x(t)\mathrm{e}^{i2\pi ft}\mathrm{d}t \quad t = 1\ldots N \quad (3)$$

with $x(t)$ as the discrete time series, f the frequency (that is $1/a$), and P as spectral power (Davis, 1986). For modeling purposes, we extracted the amplitudes A_f of the Fourier frequencies, with $n=N/2$ from the spectral power by:

$$A_\mathrm{f} = \sqrt{2P_\mathrm{f}^2/n} \quad (4)$$

The interpolations have the effect of enhancing the correlation of successive time-series data, producing artificial autocorrelation in the lag-one ('red noise') variability and suppressing the random background ('white noise') variability (e.g., Kirchner and Weil, 1998). Thus, we calculated the white-noise level (Davis, 1986) and the red-noise level from the lag-one autocorrelation coefficient according to an auto-regressive model, using the null hypothesis for significance (Mann and Lees, 1996). We calculated the 95% confidence levels based on lag-one auto-regressive models (Prokoph et al., 2000).

The differences in the nature of the time-to-wavelength transform between wavelet and spectral analysis are shown for a synthetic time series in Fig. 3. The synthetic time series includes three abrupt dis-

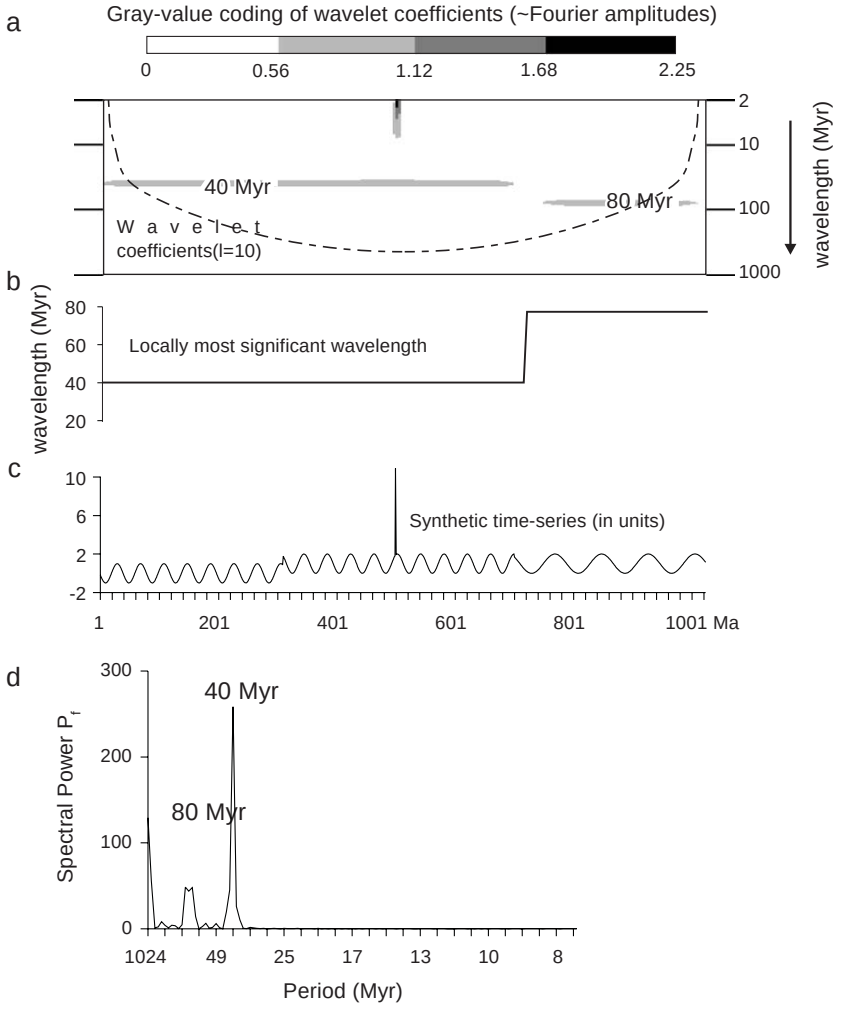

Fig. 3. Wavelet analysis of synthetic time-series signal using Morlet wavelet with $l = 10$. (a) Wavelet scalogram in which the vertical axis shows continuous spectra of possible cycle periods on a logarithmic scale, The dark gray and black areas in the scalogram mark well-pronounced cyclicity for specific time intervals. Top: Gray-scale code of wavelet coefficients that represent the amplitude of a signal at specific wavelength. The dashed line marks the boundary separating areas with significant edge effect (below) from areas with insignificant edge effects (above) = the 'cone of influence' (Torrence and Compo, 1998). (b) Most significant local wavelength (7% bandwidth uncertainty) extracted from wavelet analysis. (c) Synthetic time-series with three abrupt discontinuities at 300, 500 and 700 Myr ago of a 1-billion-year-long record. (d) Spectral analysis (fast Fourier transform) with periodogram of the model time series.

continuities at 300 Myr ago (jump in period length), 500 Myr ago (signal spike), and 700 Myr ago (jump in mean signal value), which are superimposed on periodic cycles of 80- and 40-Myr length in a 1-billion-year-long record.

Wavelet analysis is able to detect the jump in the period length and the signal spike precisely in its location, and to trace the wavelengths of the synthetic cycles through time (Fig. 3a,b). The wavelet analysis also detects the input amplitude of the cycle (top of Fig. 3a), except for small intervals at the beginning and end ('edge effects'). By contrast, Fourier analysis is not able to detect temporal discontinuities, to distinguish between continuous low-amplitude and non-stationary high-amplitude signals, or to yield information on the temporal persistence

of periodicities. Furthermore, the signal spike results in an artificial elevated power for the longest (1-billion-year) period (Fig. 3d).

Since datasets may be correlated on long time scales, but not on short time scales, and vice versa, we utilized cross-spectral analysis to identify the bandwidth-dependent correlation between the various time series (Davis, 1986). To test the confidence of the cross-spectral analysis, we carried out a squared-coherency calculation using a Hamming-window filter. Only periodicities with squared coherencies>95% confidence (one sided) at 6 degrees of freedom (DOFs) per band (Torrence and Compo, 1998) are marked in the cross-spectra.

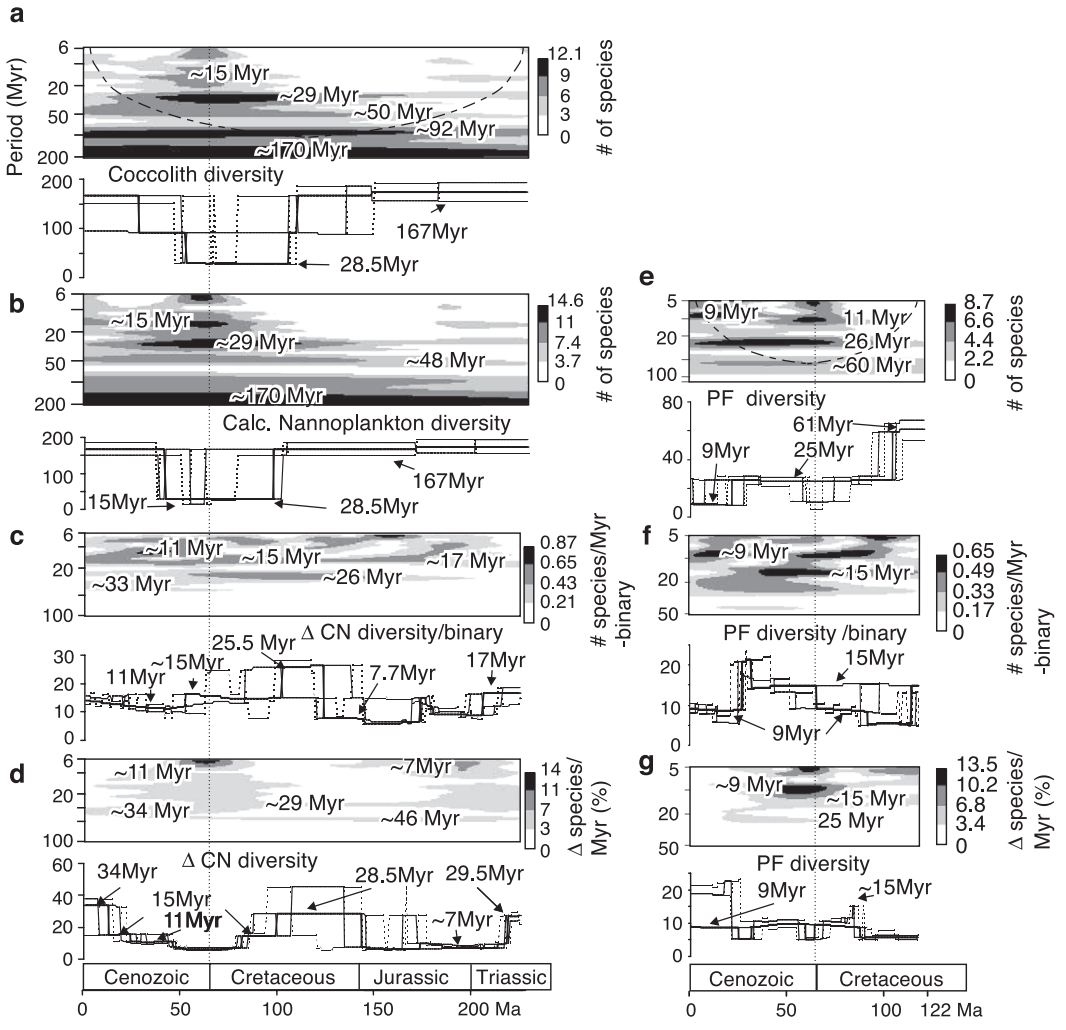

Fig. 4. Wavelet scalograms of planktonic evolutionary records (for data, see Fig. 1), time scale after Okulitch (2002). For all records (a–g), right sides: Grey-scale for Wavelet coefficients on top of scalogram coded in units of Fourier amplitudes. Tops: wavelet scalogram (for explanation, see Fig. 3a), bottoms: three most significant cycles (±7% bandwidth uncertainty) at a specific time interval, bold=primary cycle, solid=secondary cycle, dotted=tertiary cycle. Dotted vertical lines marks the K–T boundary. Dashed line at top of (a) marks the 'cone of influence' that is valid for a–d, dashed line at top of (e) marks the 'cone of influence' that is valid for e–g. Note that black and dark grey bands in the scalograms trace the wavelengths (periodicities) with the highest amplitudes.

3. Results

3.1. Trends and cyclicity in the evolution of calcareous plankton

3.1.1. Calcareous nannoplankton

The records of diversity of calcareous nannoplankton (and separately coccoliths) are characterized by long-term trends of ~ 170 and ~ 92 Myr (Fig. 4a,b), but tests show that these are not statistically significant. The most persistent (>95% significant) CN diversity cycle has a wavelength of ~ 28 to 33 ± 2.3 Myr (mean = 29 Myr) with an average amplitude of 9.5 species (ranging from 4 species in the Early Jurassic to 14 species in the mid-Cretaceous to early Cenozoic) (Figs. 4a,b and 5c). In the record of CN diversity, this ~ 29-Myr cycle is particularly significant during the Cretaceous, but is variable, with a waveband that stretches from 29 to 34 ± 2 Myr (Figs. 4d and 5b). In the binary species record of CN (which eliminates possible influences of extreme diversity changes) this cycle remains significant in the range of 25 to 33 ± 2 Myr (Figs. 4c and 5a).

Another cycle length with >95% significance for CN diversity centers at 15.3 ± 0.51 Myr (Figs. 4a–c and 5a–c). This cycle is particularly strong in the Late Triassic/Early Jurassic and during the Cenozoic, with amplitudes of 3–14 species, but with smaller amplitudes (< 3 species) throughout the Cretaceous. A similar cycle length of 11–17 Myr is very persistent in the binary CN diversity data throughout the entire 222-Myr record (Fig. 4c). Cycles of 7–11 Myr also provide a significant part of the variability in CN diversity (Fig. 5a,b), in particular during adaptive radiations and recoveries in the Early Jurassic and Early Paleogene (Fig. 4d).

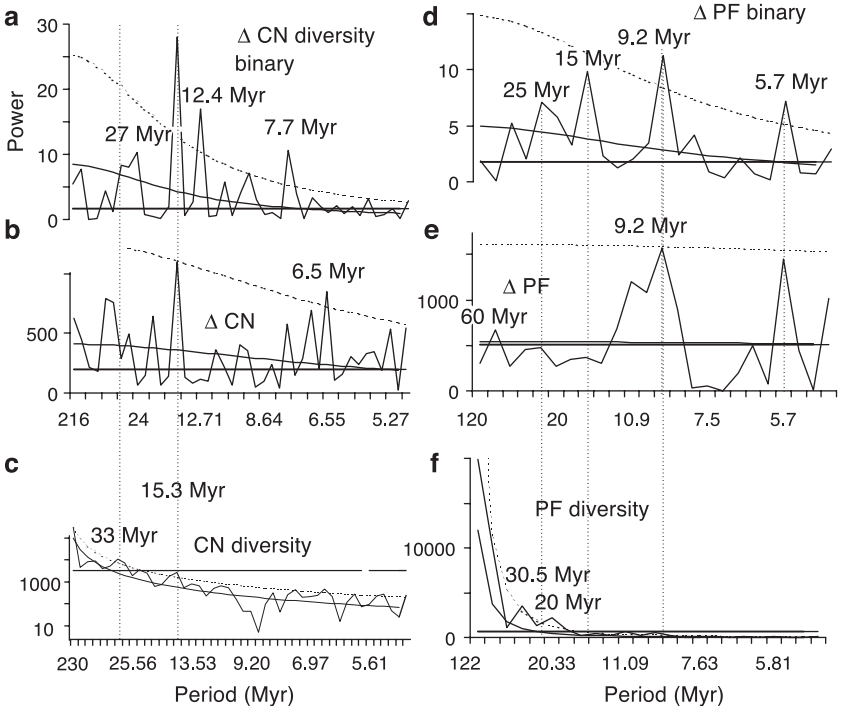

Fig. 5. Spectral analysis (Fourier analysis) of evolutionary records of calcareous nannoplankton (a–c) and planktonic foraminifera (d–f) (for data, see Fig. 1). (a–f) Power spectra (periodograms); horizontal bold lines = White noise background; continuous solid lines = red noise level from lag-one autoregressive model; dashed lines = 95% significance level from lag-one autoregressive model; vertical dotted lines = periods (wavelength) that are correlative (for details, see text).

3.1.2. Planktonic foraminifera

Cycles in the planktonic foraminifera (PF) diversity data range from 5.7 to 60 Myr (Figs. 4e–g and 5d–f). The long 60-Myr cycle is not statistically significant (Figs. 4e and 5e). A 26 ± 2 Myr cyclicity occurs persistently, however, and is significant throughout

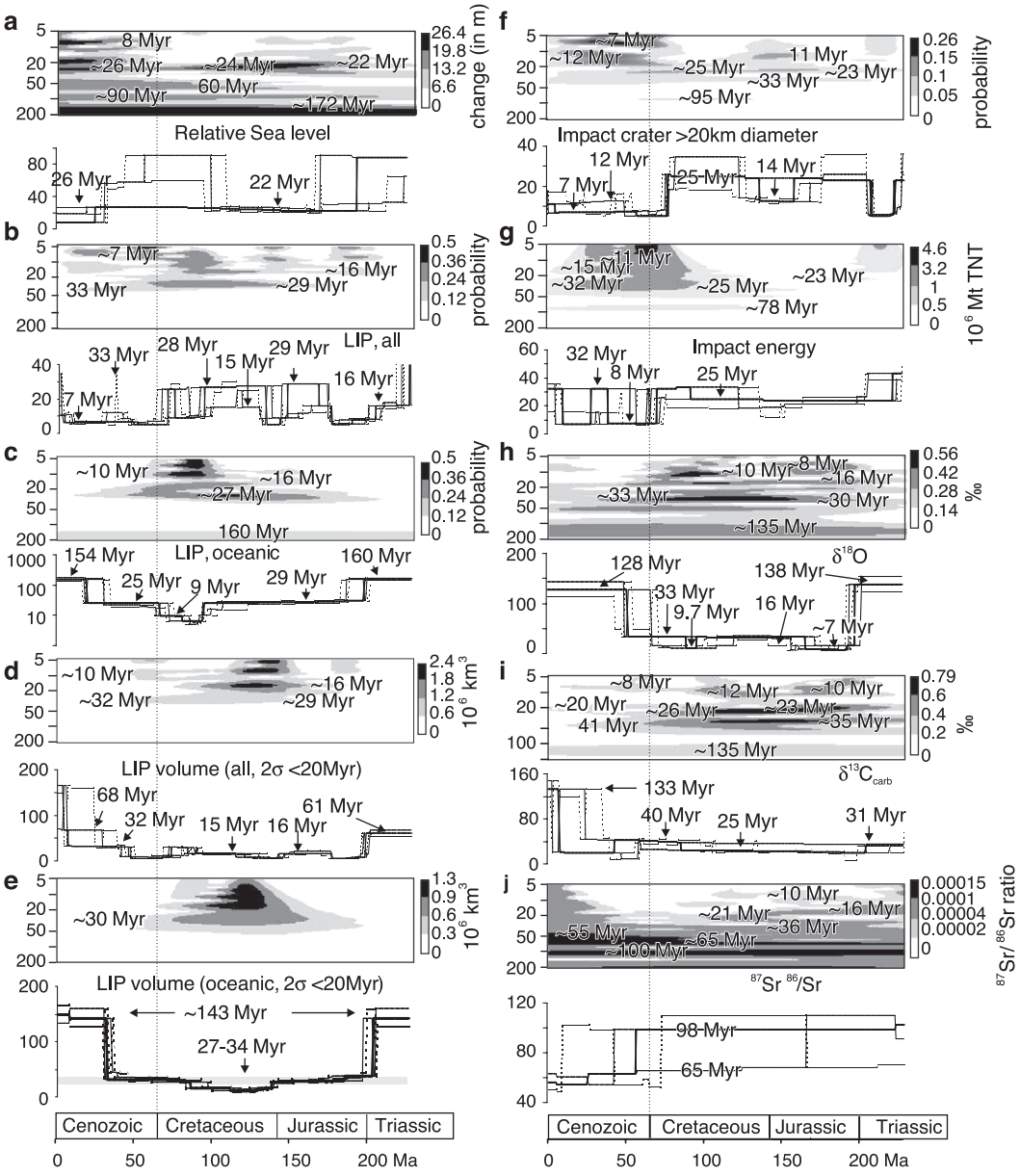

Fig. 6. Wavelet scalograms of geological records (for data, see Fig. 2), time scale after Okulitch (2002). For all records (a–g), right sides: Grey-scale for Wavelet coefficients on top of scalogram coded in units of Fourier amplitudes. Tops: wavelet scalogram (for explanation, see Fig. 3a); bottoms: three most significant cycles (± 7% bandwidth uncertainty) at specific time intervals; bold = primary cycle; solid = secondary cycle; dotted = tertiary cycle. Dotted vertical lines mark K–T boundary. For 'cone of influence', see Fig. 4a. Note that black and dark grey bands in the scalograms trace the wavelengths (periodicities) with the highest amplitudes.

the PF diversity record, with amplitudes ranging from ~ 3 to 8.7 species (average = 7.6 species) (Figs. 4e and 5d,f).

The relative changes of PF diversity (Δ species/Myr) are characterized by cycles of 9.2 ± 0.4 and 11–15 Myr (Figs. 4f,g and 5d,e). These cycles in planktonic foraminiferal diversity are not persistent, with the ~ 15-Myr cycle dominating prior to the Eocene/Oligocene boundary (34 Myr ago), and the 9-Myr cycle dominating between 34 Myr ago and the present (Fig. 4f,g). Cycles of 5.7 and ~ 11 Myr that are confined to the K/T boundary interval (Fig. 4e,g), are probably artifacts of the mathematical transform of the abrupt signal change (Figs. 4f and 5e).

3.2. Cyclicity in the geological record over the past 230 Myr

The records of geological changes exhibit several trends and cycles ranging from 6.5 to 172 Myr over the last 230 Myr (Figs. 6 and 7). The significance levels of periodic cycles longer than 90 Myr, however, are limited by edge effects in the wavelet transform (Fig. 4) and high red-noise levels (Fig. 7). The continuous relative sea level and marine-isotope records exhibit persistent cyclicity in the range of 22 ± 1.4 Myr (for sea-level change) to 36 ± 2.5 Myr (for strontium isotopes) (Fig. 6e,j), which is most often centered at ~ 26 to 33 Myr (Fig. 7a–f). The 22- to 36-Myr cyclicity in the continuous environmental records is strongest through the Jurassic and Cretaceous Periods, with amplitudes of up to ~ 26 m sea-level change (average = 12.4 m), ~ 0.5 ‰ $\delta^{18}O$ (ΔT ~ 2.5 °C according to Sellwood et al., 1994), and 0.5 ‰ $\delta^{13}C$ (average = 0.31 ‰), as illustrated in Fig. 6. Shorter cycles of 7–16 Myr occur non-persistently (Fig. 6), and with less significance over the entire record (Fig. 7).

The Large Igneous Province eruptions show a relatively persistent 27–33 Myr cyclicity in age-

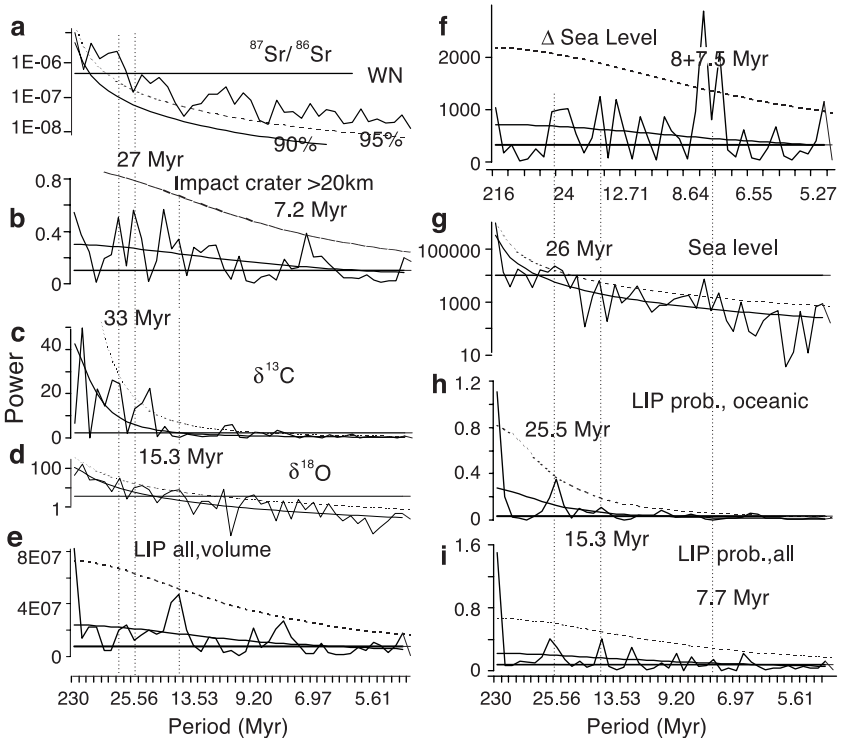

Fig. 7. Spectral analysis (Fourier analysis) of geological records (for data, see Figs. 1 and 2). (a–l) Power spectra (periodograms); horizontal bold lines = white noise background (WN); continuous solid lines = red noise level (RN) from lag-one autoregressive model; dashed lines = 95% significance level from lag-one autoregressive model; vertical dotted lines = periods (wavelength) that are correlative (for details, see text).

probability records (Fig. 6c,f), which is > 95% significant for the oceanic LIP event subset (Fig. 7h). The ages of the LIPs also show non-persistent 10–16 Myr cycle bands (Fig. 6c). When the record is transformed into more geologically relevant LIP volumes (see Fig. 2), the cyclic pattern is dominated by the very large oceanic LIP eruptions at ~ 122 Myr ago (e.g., Ontong–Java Plateau) (Fig. 6e). The amplitude of this singular event diminishes the statistical significance of any long-period cyclicity. The volume record for all LIP events is dominated by a series of large continental flood basalt eruptions, that exhibit a semi-persistent 29–32 Myr cyclicity from the Jurassic to the Paleogene, with an amplitude of 0.6 to 1.2×10^6 km^3 lava volume (Fig. 6d).

The results for the impact-crater data sets are quite similar to those derived from LIPs. The age-probability record of impact craters shows a similar 25–33 Myr cyclicity (Fig. 6f). For impact energies, the cyclic pattern is dominated by the very large Chicxulub impact at 65 Myr ago (Fig. 6g). The ages of impact craters >20 km in diameter shows a 23- to 33-Myr period, and also non-persistent 10- to 16-Myr cycle bands (Fig. 6f).

3.3. Relationships between plankton evolutionary cyclicity and geological trends and events

We used linear correlation analysis (Table 1) to determine the 95% significance of linear relationships between the planktonic diversity records (Fig. 1) and the geological time series (Fig. 2). Furthermore, we included in our analyses second-order de-trended records of diversity of coccoliths (CL_{detr}), PF (PF_{detr}) and CN (CN_{detr}) along with the de-trended record of sea-level changes (SL_{detr}), because the strong cyclic trend in the original records (see Figs. 1 and 2) tends to mask any underlying randomness or correlation. The equations for the second-order trends, with t = age in Myr are:

$CL_{detr} = CL - (-0.0059t^2 + 1.1t + 26.7)$, with a maximum in the trend line at 93.2 Myr ago,
$CN_{detr} = CN - (-0.007t^2 + 1.23t + 43.7)$, with a maximum in the trend line at 87.9 Myr ago,
$PF_{detr} = PF - (-0.0005t^2 + 0.51t + 62.7)$, with no maximum in the last 122 Myr,
$SL_{detr} = SL - (-0.0121t^2 + 2.34t + 52.4)$, with a maximum in the trend line at 96.7 Myr ago.

Table 1
Linear correlation between plankton fossil records and geological records

	PF	$PF_{detr.}$	ΔPF	CL	$CL_{detr.}$	CN	$CN_{detr.}$	ΔCN
$PF_{detr.}$	**0.52**	×						
ΔPF	−0.28	**−0.34**	×					
CL	**−0.39**			×				
$CL_{detr.}$		0.28		**0.48**	×			
CN	**−0.42**			**0.97**	**0.39**	×		
$CN_{detr.}$				**0.42**	**0.92**	**0.41**	×	
ΔCN				−0.23		−0.24		×
Sea level	**−0.58**			**0.79**		**0.82**		
$SL_{detr.}$	−0.28			0.24	**0.39**	**0.28**	**0.49**	
Impact (km)			**−0.39**					**−0.32**
Impact (Mt)			**−0.48**					**−0.42**
$^{87}Sr/^{86}Sr_{carb}$	**0.74**							
$\delta^{18}O_{carb}$	**0.61**				**−0.36**		**−0.4**	
T (°C)	**−0.56**				**0.43**		**0.46**	
$\delta^{13}C_{carb}$	**−0.62**						0.22	
LIPoc (volume)	**−0.35**							
LIPall (volume)	−0.28		−0.23					
LIPall (probability)	**−0.29**			**0.3**		**0.29**		
LIPoc (probability)	**−0.38**			**0.44**		**0.43**		
Impact > 5 km			−0.23					**−0.28**
Impact > 20 km			−0.24					**−0.28**

Bold = 95% confident, two-sided; fine = 95% confident, one-sided.

The linear-correlation analysis suggests that the diversity of planktonic foraminifera is negatively correlated with the diversity of calcareous nannoplankton. PF diversity is also negatively correlated with high sea level, global ocean temperatures, and large volumes and age probabilities of LIP events (Table 1). The detrended planktonic foraminiferal record does not show these latter correlations, suggesting that the general increasing trend in foraminiferal diversity is independent of long-term sea level and the LIP eruption history. The relative changes of planktonic foraminiferal diversity (ΔPF/Myr) are significantly negatively correlated with impact events (diameter, energy and age probability) and to the volume of magma in LIP events (Table 1), suggesting that these energetic geologic events lead to extinctions of planktonic foraminifera.

The linear correlations of the diversity of calcareous nannoplankton (CN) and coccoliths (CL) with the geological record differ from those of planktonic foraminifera. In particular, CN and CL diversity (and their de-trended records) correlate significantly positively with sea level (both non-de-trended and de-

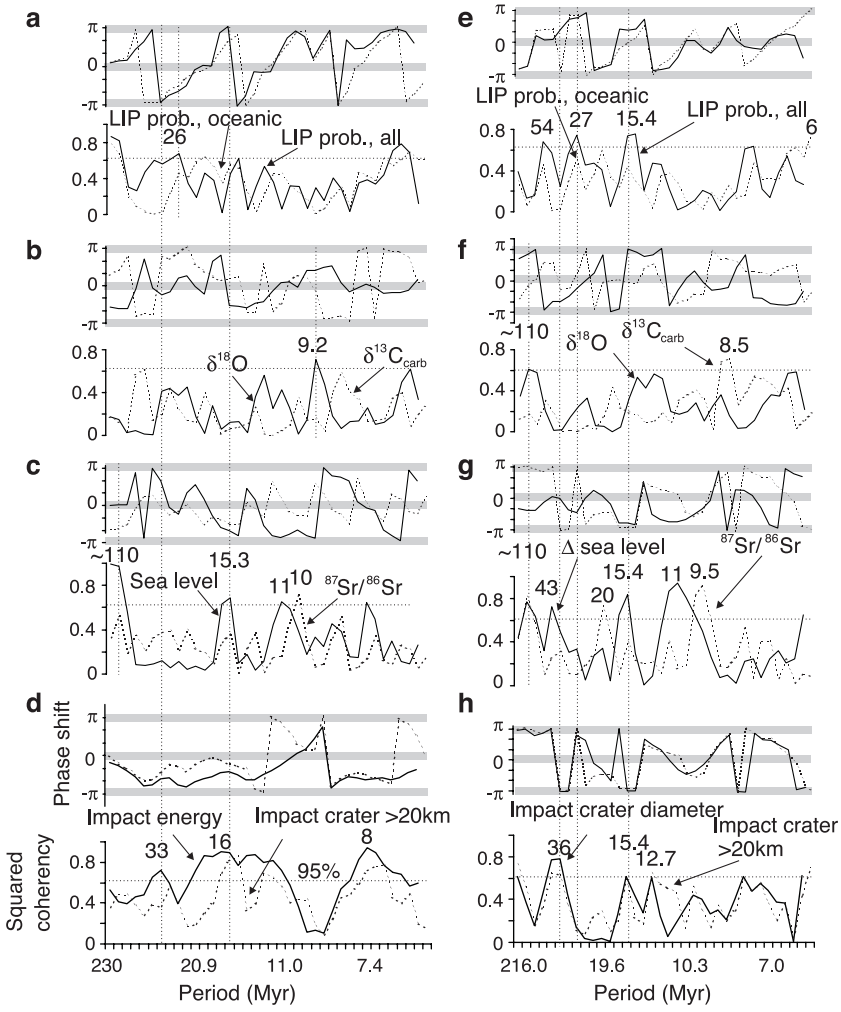

Fig. 8. Cross-spectral analysis of evolutionary records of calcareous nannoplankton (CN) with geological records, (a–d) CN diversity with over the last 230 Ma: (e–f) change of CN diversity (in %) with geological records over the last 216 Ma. Squared coherencies on top and phase spectra (+3.14 to −3.14 radians) at top. Vertical dotted lines = periods with significant cross-correlation; horizontal gray bars mark in-phase or 90° (+π, −π) off-phase cross-correlation ranges; horizontal dotted line = 95% (one-sided) confidence levels for 6 DOF (for details, see text).

trended), and with the LIP volcanic events (Table 1). The relative changes of CN diversity (ΔCN/Myr), however, are negatively correlated with the size and probability of impact events, suggesting that impact events>5 km are a common cause for extinction of calcareous nannoplankton, with recovery times lasting more than 1 Myr.

Cross-spectral analysis (Figs. 8 and 9) recognized a variety of periods (cycle lengths) in which the CN and PF diversity records are significantly correlated (i.e., high squared coherencies) with the geological records. Here, we focus on the periods that were shown to be persistent (see Figs. 3 and 4) and significant in each record (Figs. 5 and 6). Furthermore, the significant, and in-phase (0 radians) cross-correlation of the CN diversity records with sea level and LIP events (Fig. 8a, c) verifies the linear correlation analysis for the overall trend summarized

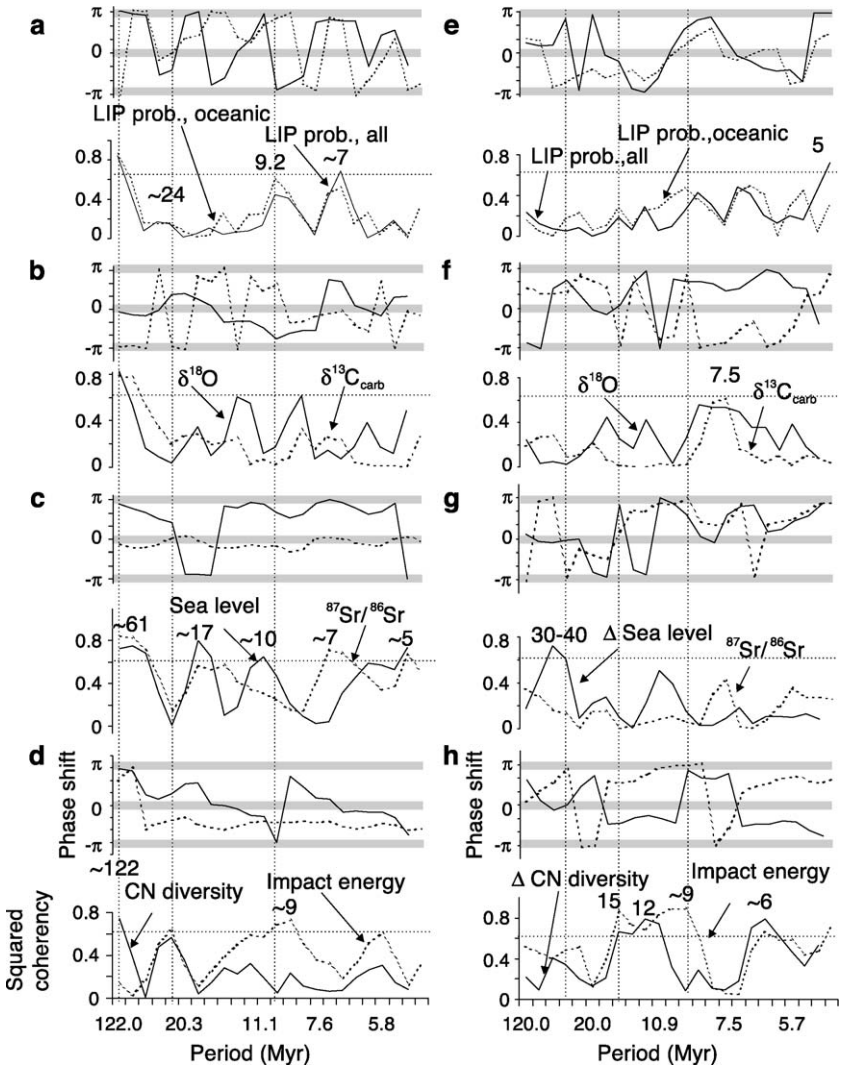

Fig. 9. Cross-spectral analysis of evolutionary records of ploanktonic foraminifera (PF) with geological records, (a–d) PF diversity with records over the last 122 Ma: (e–f) change of CN diversity (in %) with geological records over last 120 Ma. Squared coherencies on top and phase spectra (+3.14 to −3.14 radians) at the top. Vertical dotted lines: periods with significant cross-correlation; horizontal gray bars mark in-phase or 90° (+π, −π) off-phase cross-correlation ranges; horizontal dotted line = 95% (one-sided) confidence levels for 6 DOF (for details, see text).

above (Table 1). When Eq. (4) is applied to the spectral values of calcareous nannoplankton diversity and of sea level (Figs. 3 and 4), a second-order cycle of CN diversity with an amplitude of ~ 51 species over the last 220 Myr and peak at ~ 92 Myr ago corresponds to a similar sea-level cycle with an amplitude of 90 m (ΔSL). Consequently, an ~ 1.8 m global sea-level fall corresponds, on average, to a diversity decrease of one CN species.

The ~ 30 Myr cyclicity (22–36 Myr band) is significantly inversely cross-correlated between the CN records and the impact-cratering records (Fig. 8d,h), with a −2.96 radians (−14 Myr) phase shift for impact crater (>20 km) age probability and crater size (Fig. 8, top of h). The CN diversity and ΔCN/Myr are similarly inversely cross-correlated with the LIP records in the 26–33 Myr band (Fig. 8a,e), but are −2.5, −3.1, and +2.8 and +2.9 radians (i.e., 10 to 12 Myr) phase shifted. Changes in sea level and in isotope records are not significantly cross-correlated with the CN records at the 22- to 36-Myr wavelengths (Fig. 8b,c,f,g). The 15.3 ± 0.5 Myr cycle band of the ΔCN/Myr record is significantly inversely cross-correlated with the impact cratering records, sea level, and the LIP event records (Fig. 8a,c,d,e,g,h), but not with the isotope records.

For wavelengths and trends >61 Myr long, the PF diversity is also significantly but +2.9 radians out-off phase (i.e., negatively) cross-correlated with relative sea level (Fig. 9c). For the ~ 30-Myr (22–36 Myr) cycle band, there is no significant cross-correlation between the PF records and the geological records, except for a significant positive correlation of the ΔPF/Myr record with the Δsea level record (i.e., decreasing relative PF diversity is correlated with decreasing relative sea level). For the 12–17 Myr cycle band, there is only a 1.67 radians (~ 4 Myr) out-of-phase cross-correlation between ΔPF/Myr and impact energy. The PF records of the ~ 9 Myr waveband are significantly negatively cross-correlated with the oceanic LIP probability and the impact cratering record (Fig. 9a,h).

In summary, (1) A ~ 29-Myr (22–36 Myr) cycle band dominates in all of the records of planktonic diversity and of geological change; (2) a ~ 15 Myr cycle is significant in the CN diversity records; and (3) a ~ 9 Myr cycle is significant in the PF diversity records (Table 2). For example, the amplitude of

Table 2
Planktic evolutionary cycle amplitudes and phase shifts to geological records

Cycle length	25.5–32.9 Myr		15.3 Myr		9.2 Myr	
Bandwidth uncertainty	± 2.3		± 0.51		± 0.35	
	Amplitudes (average)	Phase shift with CN	Amplitudes (average)	Phase shift with CN	Amplitudes (average)	Phase shift with PF
CN diversity	9.5 species	×	4.8 species	×	1 species	−4.5 Myr
ΔCN	6.2%	N/A	3.20%	N/A	1.80%	3.7 Myr
ΔCN binary	0.28	N/A	0.68	N/A	0.26	N/A
Sea level	12.4 m	−0.6 Myr	7.3 m*	−4.9 Myr*	3.3 m*	3.1 Myr*
Impact energy	2.6×10^6 Mt TNT	−19 Myr	2.4×10^6 Mt TNT	−6.4 Myr	2.1×10^6 Mt TNT	−2.1 Myr
Impact crater > 20 km	0.056*	−14 Myr*	0.054*	−6.8 Myr*	0.01	4.2 Myr
$\delta^{18}O$	0.32‰	−3.7 Myr	0.26‰	−7.4 Myr	0.2‰	−3.4 Myr
Ocean temperature	1.7 °C	12.4 Myr	1.1 °C	7 Myr	0.7 °C	0.45 Myr
$\delta^{13}C_{carb}$	0.31‰	12.6 Myr	0.046‰	3 Myr	0.15‰	2.9 Myr
$^{87}Sr/^{86}Sr$	0.00008	−0.7 Myr	0.000016	−7 Myr	0.00001	−0.7 Myr
LIP prob., oceanic	0.05	−6 Myr	0.03	4.7 Myr	0.005*	4 Myr*
LIP prob., all	0.04*	−10 Myr*	0.059*	7.5 Myr*	0.035	−2.6 Myr
LIP volume, all	404 km^3	−11 Myr	641 km^3*	7.5 Myr*	433 km^3	−4 Myr
LIP volume, oceanic	451 km^3*	−10 Myr*	342 km^3	6.8 Myr	133 km^3	4 Myr
PF diversity	7.6 species	−2.39	2.1 species	0 Myr	3 species	×
ΔPF	2.8 %	N/A	2.50%	N/A	5.10%	N/A
ΔPF binary	0.25	N/A	0.4	N/A	0.43	N/A

* Statistically significant at >95% confidence level.

the ~ 29 Myr cycle of calcareous nannoplankton diversity is on average 9.5 species (range: 4–14 species, see Fig. 3), corresponding to amplitudes of 7.6 planktonic foraminifera species, 12.4 m sea level change, or 1.7 °C ocean surface temperature (Table 2). However, the ~ 29, ~ 15, and ~ 9 Myr cyclicities are not necessarily cross-correlated between the planktonic diversity and geological records (Table 2) as shown by the cross-spectral analysis.

Based on the statistical results, we were able to construct best fit stationary-periodic models for the diversity records of PF and CN (with t = time in Myr):

$$\text{CN diversity} = 9.5\ \sin(2\pi(t - 7.5\ \text{Myr})/29\ \text{Myr}) + 4.8\ \sin(2\pi(t - 4\ \text{Myr})/15.3\ \text{Myr}),$$

$$\text{PF diversity} = 7.6\ \sin(2\pi(t - 12\ \text{Myr})/26\ \text{Myr}) + 3\ \sin(2\pi t/9.2\ \text{Myr}).$$

These models are able to describe major patterns in the diversity history of calcareous plankton, such as: (1) the sawtooth-shaped ~ 29 Myr cycle in the diversity of

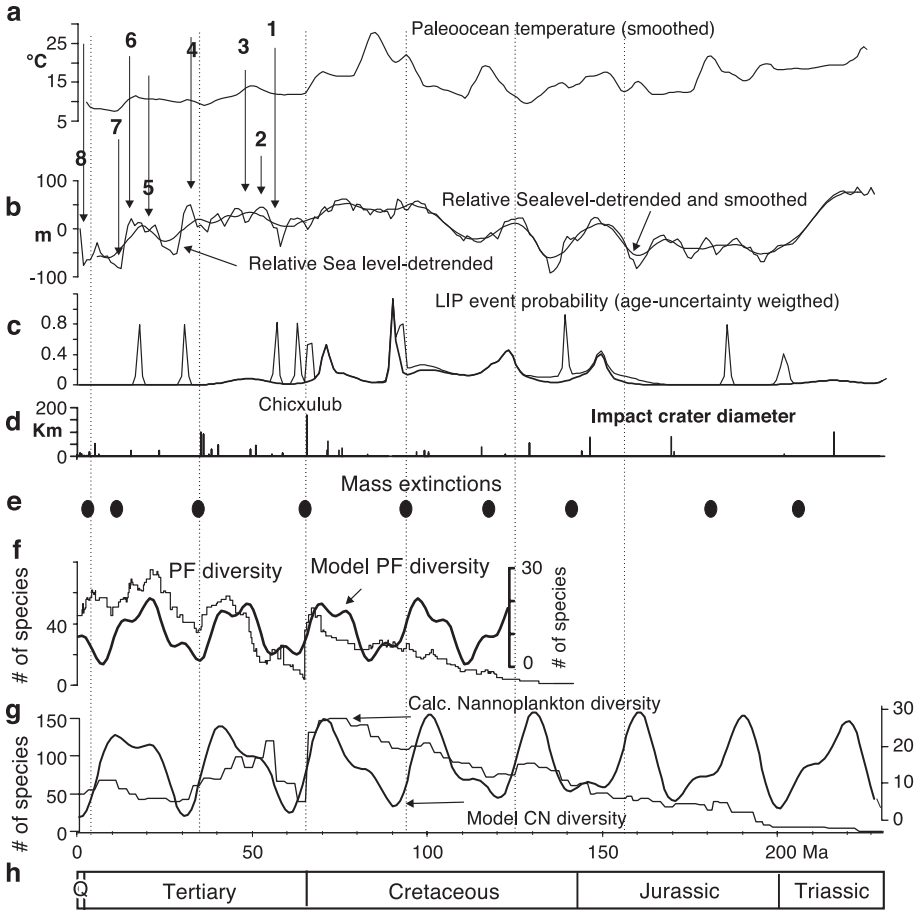

Fig. 10. Periodic cyclic model of the long-term response of the diversity of calcareous nannoplankton (CN) and planktonic foraminifera (PF) to forcing by periodic geological and environmental changes. Ocean paleotemperatures calculated according to Sellwood et al. (1994) from oxygen-isotope data (Fig. 2), with corrections of −1‰ for the pre-Oligocene record according to Shackleton and Kennett (1975). Mass extinctions after Raup and Sepkoski (1986). Tertiary climatic record after Pearson and Palmer (2000): 1: Late Paleocene thermal maximum ~ 55 Ma; 2: Early Eocene climate optimum ~ 54 to 50 Ma; 3; Early mid-Eocene cooling ~ 50 to 45.5 Ma; 4: major ice growth on Antarctica ~ 33 Ma; 5: Early Miocene glaciation ~ 22 Ma; 6: mid-Miocene climate optimum ~ 17 Ma; 7: expansion of East Antarctic ice sheet ~16 to 14 Ma, 8: Northern Hemisphere glaciation ~ 4 to 2 Ma (vertical dashed lines for graphic correlation assistance).

Table 3
~ 15-Myr intervals of planktic evolutionary change and geological events

Model	Impact cratering			LIP			PF change/Myr		CN change/3 Myr	
Age (Ma)	Age (Ma)	Size (km)	Crater name	Age (Ma)	Size V (km^3)	Name	Age (Ma)	%	Age (Ma)	%
5	< 5	52	Kara–Kul				3/4	− 7	3.5/6.5	− 19
20	23 ± 1	24	Haughton	17 ± 1	175	Columbia	20/21	− 6	18.5/21.5	0
35	35.5 ± 0.3/ 35.7 ± 0.2	90/100	Chesapeake Bay/Popigai	30 ± 1	1200	Afar	35/36	− 16	33.5/36.5	− 15
50	50.50 ± 0.76	45	Montagnais	48 ± 10/ 56 ± 1	100/ 7900	Metchosin/ NAVP	50/51	19	48.5/51.5	− 12
65	64.98 ± 0.05	170	Chicxulub	65.5 ± 1	8600	Deccan	64/65	− 85	63.5/69.5	−69
80							80/81	0	78.5/81.5	− 1
95	95 ± 7	25	Steen River	95 ± 10	2000	Alpha	93/94	− 13	93.5/96.5	− 4
110	115 ± 10	39	Carswell	111 ± 10	900	Nauru	110/111	− 10	108.5/111.5	1
125	128 ± 5	55	Tookoonooka	122 ± 3	38400	Ontong	124/125	0	123.5/126.5	− 16
140	142.0 ± 2.6	40	Mjolnir	138 ± 1	23000	Paraná–Etendeka			141.5/144.5	− 5
155				155 ± 10	300	Argo			153.5/156.5	− 2
170	167 ± 3	80	Puchezh–Katunki						168.5/171.5	21
185				184 ± 1	10000	Karoo–Ferrar			183.5/186.5	− 28
200				200 ± 1	2000	CAMP			198.5/201.5	44
215	214 ± 1	100	Manicouagan	214 ± 14	450	Angayucham			213.5/216.5	25

Bold = 30-Myr interval.

calcareous nannoplankton, with gradual increase and abrupt fall of diversity; (2) The plateau-shaped ~ 26 Myr cycles in the planktonic foraminifera record, with abrupt diversity increases and decreases; and (3) The modulation of the shape of the 26–29 Myr cycle by the ~ 15.3- and 9.2-Myr periodic components (Fig. 10). The periodic evolutionary models proposed do not fit the early records of diversity (e.g., the first ~ 70 Myr of calcareous nannoplankton and the first ~ 50 Myr of planktonic foraminifera evolution), perhaps because early species were less affected by periodic environmental changes, or as a result of the relatively poor early diversity record.

The planktonic diversity records and best-fit models correlate less well with the record of sea-level change and ocean paleotemperatures. For impact cratering, 11 of the 14 largest impact craters (and all of the five largest) fit a 15-Myr periodic model (Table 3). In particular, the ~ 30 Myr spaced impact structures (e.g., Kara, Chesapeake Bay/Popigai, Chicxulub, Steen River and Tookoonooka) correspond well (± 3 Myr age uncertainty range) with major plankton extinction intervals (Table 3). Twelve out of fifteen ~ 15 Myr spaced extinction intervals also correspond to LIP volcanic events. The large-volume LIP events (>10^6 km^3) tend to correlate with major planktonic extinction intervals, particularly those involving calcareous nannoplankton (Table 3), supporting the results of our time-series analysis (Fig. 8e, Table 2).

4. Discussion of results

Our results suggest that the diversity of planktonic foraminifera (PF) and calcareous nannoplankton (CN) over the past 230 Myr have followed a pattern involving ~ 28 to 32 Myr cycles. The diversity records of the two planktonic groups are phase-shifted (by ~ 2 to 3 Myr) (e.g., see Fig. 2). The dominant ~ 30 Myr cycle is modulated by ~ 15 and ~ 9 Myr cycles, which affect the shapes of the ~ 30 Myr peaks. LIP events and impact cratering in the ~ 30 and ~ 15 Myr cycle bands are well correlated with the planktonic evolutionary records. In both the PF and CN records, the amplitude of the proposed ~ 15 Myr (12–17 Myr) cycle is only about half of that of the ~ 30 Myr cycle, but extinction events with this ~ 15 Myr spacing fit well with the spacing of several large LIPs and impact

events. Previous studies (e.g., Prokoph et al., 2001) have shown that even after the removal of the extreme diversity decreases at 65 and ~ 34 Myr ago, the ~ 30 Myr and ~ 15 Myr periodicities are well represented in the planktonic foraminifera record. It is noteworthy that the times of low PF and CN diversity predicted by the periodic models agree with the times of significant marine mass extinction events identified by Raup and Sepkoski (1986).

The correlation analyses indicate that diversity of calcareous nannoplankton decreased at times of ocean-temperature cooling and sea-level fall. This can be seen clearly in the case of the major Cenozoic climate episodes (Pearson and Palmer, 2000; Zachos et al., 2001) (Fig. 10). It would be possible that the oxygen and carbon isotope records exhibit random linear correlations with the plankton records, because of interpolations and mix of data from different environments in the isotope records. However, the correlation found here is significant only between $\delta^{18}O$ and the detrended CN record (Table 1) and at ~ 33 and ~ 9.2 Myr periodicities (Fig. 8c). By contrast, the diversity of planktonic foraminifera was reduced during LIP eruptions (Tables 1 and 3; Fig. 10). The PF diversity decreased or was subject to significant turnovers during mid-Cretaceous anoxic events, which may be closely linked to LIP eruptions (Leckie et al., 2002).

Our results also suggest that the largest asteroid and comet impacts have significantly affected the diversity of calcareous marine plankton since the Late Triassic. For example, the diversity of both planktonic foraminifera and calcareous nannoplankton underwent drastic reductions at the K/T boundary event (see Fig. 1). The recovery of diversity seems to have been independent of sea-level fluctuations, in a partly self-organized process (e.g., Prokoph et al., 2000), until the late Paleocene (~ 55 Myr ago). By that time, PF diversity recovered to ~ 80% of pre-K/T boundary values, and ~ 1 Myr later CN diversity climbed to a level of ~ 50% of pre-K/T boundary diversity (Fig. 1), which apparently saturated the available niche space. The generally cooler climate and lower sea levels during the earliest Tertiary reduced the area of warm surface waters as compared with the Late Mesozoic (Fig. 2), and probably contributed to the incomplete recovery of CN diversity after the K/T extinction event. A somewhat similar scenario marked the Late Eocene to Early Oligocene (~ 35 to 31 Myr ago), with a recovery interval for CN that lasted ~ 7 Myr (see Figs. 1 and 10).

We have found a consistent, although a rather weak, relationship between the cyclicity (in particular the ~ 30 Myr periodicity) in long-term plankton evolution and in the marine-isotope records. One reason for the weak correlation could be that marine isotopic composition usually recovers from major events in less than ~ 500 kyr, as shown for the Cretaceous/Tertiary boundary (Caldeira and Rampino, 1993), the Permian/Triassic boundary (e.g., Rampino et al., 2000; Berner, 2002) and Early Aptian events (e.g., Leckie et al., 2002), whereas recovery of planktonic diversity requires a significantly longer time. In addition, the marine isotope database (Veizer et al., 1999) is still relatively sparse for the Late Cretaceous (~ 90 to 76 Ma), and made problematic in general by its non-homogeneity, utilizing mainly benthic organisms in the Cenozoic, mainly planktonic fossils in the Late Cretaceous, and mainly nektonic fossils from the Late Triassic to Early Cretaceous. In particular, the mixing of 'cooler' benthic foraminifera data with 'warmer' PF data for the last ~ 65 Myr (Veizer et al., 1999) is probably responsible for the weakening of the high-frequency fluctuations that have been evident in purely benthic records (e.g., Shackleton and Imbrie, 1990). Eventually, a higher-resolution (e.g., < 500 kyr) and paleobiologically more consistent database might uncover significant long-term relationships. At present, such a resolution and consistency is only possible on a regional scale or over relatively short time intervals (e.g., Zachos et al., 2001).

5. Interpretations and conclusions

The results of our statistical analyses suggest that there exists a basic rhythm of about 30 Myr that seems to permeate Earth history in geologic time series ranging from global sea level and climate to large-scale volcanism and large-body impacts (Fig. 10). This cycle and its modulation by weaker 15- and 9-Myr components, is also recorded in the diversity of calcareous plankton, suggesting that the diversity variations are forced by periodic or quasi-periodic geologic phenomena.

A number of previous studies have detected similar periods in various time series related to biotic diversity (e.g., Raup and Sepkoski, 1986), and geologic events (e.g., Rampino and Stothers, 1984a,b; Rampino and Caldeira, 1993; Liritzis, 1993; Stothers, 1993a,b; Negi et al., 1990, 1996).

The origin of the periodic components detected could lie either within the Earth or outside of it, or may represent a combination of terrestrial and extraterrestrial causation. Several possible mechanisms have been suggested.

5.1. Mantle plume activity

Loper et al. (1988), for example, suggested that mantle plume activity might occur with an ~22 Myr periodicity considering the thermal relaxation time related to an upper D'' layer thickness of about 11 km and a thermal diffusivity of about 1.7 m^2/s. Varying these parameters somewhat could provide periodicities in the range of ~15 to 30 Myr for mantle plume generation, and corresponding LIP events and pulses of ocean-floor spreading.

Oceanic LIP events and coincidental intense mid-ocean rifting may have influenced ocean oxygenation and stratification, at least during the mid-Cretaceous (Kerr, 1998). The abrupt ocean-temperature increases, and possible intensified nutrient upwelling and increased marine productivity that are proposed to accompany oceanic LIP eruptions may have caused O_2 depletion in the deeper ocean (Vogt, 1989) leading to PF extinction (e.g. Hart, 1990).

Another possibility is that LIP eruptions lead to large releases of SO_2 and dust that form aerosol clouds. This could cool the climate, reduce photosynthetic activity and produce acid rain (e.g., Rampino and Self, 1992). However, the correlations between LIP events and PF extinction (Table 3) are still questionable due to uncertainties of some LIP initiation ages (e.g., Ontong–Java oceanic LIP).

5.2. Large-body impacts

Several extraterrestrial mechanisms for generating an ~30-Myr cycle of large impacts have been proposed (e.g., Smolukowski et al., 1986). For example, $\sim 32 \pm 3$ Myr periodicity of comet bombardment may result from disturbances of the Oort cloud comets during our solar system's crossing of the galactic plane (e.g., Rampino and Stothers, 1984a; Matese et al., 1995,1998; Rampino et al., 1997; Rampino, 2002). Napier (1998) proposed a related galactic mechanism for generating an additional ~15 Myr cycle of impact cratering on Earth. We note that the phase of the periodic models of PF and CN diversity (Fig. 10) matches that of the galactic plane-crossing cycle. It is also of interest that the longer 160- to 170-Myr period detected in the diversity of calcareous nannoplankton, and in the records of global sea level and LIP episodes is close to the longer epicycle time related to the revolution of the solar system around the Galaxy (estimated at ~160 to 180 Myr) (Bailey et al., 1990; Matese et al., 1995).

The diversity records utilized here provide a limited, but robust view of the evolutionary pattern of calcareous plankton. Records of extinction, speciation, and rates of diversification and biotic turnover of these groups could provide additional information on evolutionary history. However, these records are by their very nature composed of discrete events, and their time-series analyses are therefore very sensitive to age uncertainties.

Although statistical analysis cannot determine the causes of the periodic components detected in this study, cyclical mantle processes and related magmatic activity, and periodic impact events seem to be major causes of environmental fluctuations that influenced the long-term evolution of life. More complete and accurate records of diversity, paleoenvironmental changes and geological events should provide further insights into the time structure of the geologic record and the potential links between astronomical, geological and biological evolutionary processes in Earth history.

Acknowledgements

We thank Paul Bown and Tim Patterson for providing hitherto unpublished data, and Ken Caldeira, Anthony Fowler and Mark Leckie for constructive discussions. We also thank Isabella Premoli-Silva and an unidentified reviewer for their critical and helpful reviews.

References

Agterberg, F.P., 1994. Estimation of the geological time scale. Mathematical Geology 26, 857–876.

Appenzeller, C., Stocker, T.F., Anklin, M., 1998. North Atlantic oscillation dynamics recorded in Greenland ice cores. Science 282, 446–449.

Bailey, M.E., Clube, S.V.M., Napier, W.M., 1990. The Origin of Comets. Pergamon, Oxford.

Berner, R.A., 2002. Examination of hypothesis for the Permo–Triassic boundary extinction by carbon cycle modeling. Proceedings of the National Academy of Sciences United States of America 99, 4172–4177.

Bolton, E.W., Maasch, K.A., Lilly, J.M., 1995. A wavelet analysis of Plio–Pleistocene climate indicators: a new view of periodicity evolution. Geophysical Research Letters 22, 2753–2756.

Bown, P.R., Burnett, J.A., Gallagher, L.T., 1992. Calcareous nannoplankton evolution. Memorie di Scienze Geologiche 43, 1–17.

Bralower, T.J., Fullagar, P.D., Paull, C.K., Dwyer, G.S., Leckie, R.M., 1997. Middle Cretaceous strontium isotope stratigraphy of deep sea sections. Geological Society of America Bulletin 109, 1421–1442.

Caldeira, K., Rampino, M.R., 1993. The aftermath of the K/T boundary mass extinction: biogeochemical stabilization of the carbon cycle and climate. Paleoceanography 8, 515–525.

Chapman, C.R., Morrison, D., 1989. Cosmic Catastrophes. Plenum, New York.

Courtillot, V.E., Renne, P.R., 2003. On the ages of flood basalt events. Comptes Rendus Geoscience 335, 113–140.

Davis, J.C., 1986. Statistics and Data Analysis in Geology. Wiley, New York.

Ernst, R.E., Buchan, K.L., 2001. Large mafic magmatic events through time and links to mantle plume heads. In: Ernst, R.E., Buchan, K.L. (Eds.), Mantle Plumes: Their Identification Through Time. Geological Society of America Special Paper, vol. 352, pp. 483–575.

Gradstein, F.M., Ogg, J.G., 1996. A Phanerozoic time scale. Episodes 19 (1,2).

Grieve, R.A.F., 1997. Extraterrestrial impact events: the record in the rocks and the stratigraphic column. Palaeogeography, Palaeoclimatology, Palaeoecology 132, 5–23.

Grossman, A., Morlet, J., 1984. Decomposition of Hardy functions into square integrable wavelets of constant shape. SIAM Journal of Mathematical Analysis 15, 732–736.

Hardenbol, J., Thierry, J., Farley, M.B., Jaquin, T., de Graciansky, P.-C., Vail, P.R., 1998. Mesozoic and Cenozoic sequence chronostratigraphic chart. In: De Graciansky, P.-C., Hardenbol, J., Jacquin, T., Vail, P. (Eds.), Mesozoic–Cenozoic Sequence Stratigraphy of European Basins. SEPM, Special Publication, vol. 60.

Hart, M.B., 1990. Major evolutionary radiations of the planktonic foraminiferida. Systematics Association Special Volume 42, 59–72.

Kerr, A.C., 1998. Oceanic plateau formation: a cause of mass extinction and black shale deposition around the Cenomanian–Turonian boundary? Journal of Geological Society London 155, 619–626.

Kirchner, J.W., Weil, A., 1998. No fractals in fossil extinction statistics. Nature 395, 337–338.

Leckie, R.M., Bralower, T.J., Cashman, R., 2002. Oceanic anoxic events and plankton evolution: biotic response to tectonic forcing during the mid-Cretaceous. Paleoceanography 17, 1301–1329.

Liritzis, I., 1993. Cyclicity in terrestrial upheavals during the Phanerozoic Eon. Quarterly Journal of Royal Astronomical Society 34, 251–260.

Loper, D.E., McCartney, K., Buzyna, G., 1988. A model of correlated episodicity in magnetic-field reversals, climate, and mass extinctions. Journal of Geology 96, 1–15.

Mann, M.S., Lees, J.M., 1996. Robust estimation of background noise and signal detection in climatic time series. Climatic Change 33, 409–445.

Matese, J.J., Whitman, P.G., Innanen, K.A., Valtonen, M.J., 1995. Periodic modulation of the Oort Cloud comet flux by the adiabatically changing galactic tide. Icarus 116, 255–268.

Matese, J.J., Whitman, P.G., Innanen, K.A., Valtonen, M.J., 1998. Variability of the Oort comet flux: can it be manifest in the cratering record? Highlights in Astronomy 11A, 252–256.

Mundil, R., Metcalfe, I., Ludwig, K., Renne, P., Oberli, F., Nicoll, R., 2001. Timing of the Permian–Triassic biotic crisis: implications from new zircon U/Pb age data (and their limitations). Earth and Planetary Science Letters 187, 131–145.

Napier, W.M., 1998. NEOs and impacts: the galactic connection. Celestial Mechanics and Dynamical Astronomy 69, 59–75.

Negi, J.G., Tiwari, R.K., Rao, K.N.N., 1990. 'Clean' spectral analysis of long-term sea-level changes. Terra Nova 2, 138–141.

Negi, J.G., Tiwari, R.K., Rao, K.N.N., 1996. Clean periodicity in secular variations in dolomite abundance in deep-marine sediments. Marine Geology 133, 113–121.

Okulitch, A.V., 2002. Geological time chart, 2002. Geological Survey of Canada, Open File 3040 (National Earth Science Series, Geological Atlas).

Palfy, J., Mortensen, J.K., Carter, E.S., Smith, P.L., Friedman, R.M., Tipper, H.W., 2000a. Timing the end-Triassic mass extinction: first on land, then in the sea? Geology 28, 39–42.

Palfy, J., Smith, P.L., Mortensen, J.K., 2000b. A U–Pb and $^{40}Ar/^{39}Ar$ time scale for the Jurassic. Canadian Journal of Earth Sciences 37, 923–944.

Patterson, R.T., Fowler, A.D., Huber, B.T., in press. Evidence of Hierarchical Organization in the Planktic Foraminiferal Evolutionary Record. Journal of Foraminiferal Research.

Pearson, P.N., Palmer, M.R., 2000. Atmospheric carbon dioxide concentrations over the past 60 million years. Nature 406, 695–699.

Prokoph, A., Fowler, A.D., Patterson, R.T., 2000. Evidence for periodicity and nonlinearity in a high-resolution fossil record of long-term evolution. Geology 28, 867–870.

Prokoph, A., Fowler, A.D., Patterson, R.T., 2001. Periodically forced self-organization in long term evolution of planktic foraminifera. Canadian Journal of Earth Sciences 38, 299–314.

Rampino, M.R., 2002. Role of the galaxy in periodic impacts and mass extinctions on the Earth. Geological Society of America Special Paper 356, 667–678.

Rampino, M.R., Caldeira, K., 1993. Major episodes of geological change: correlations, time structure, and possible causes. Earth and Planetary Science Letters 114, 215–227.

Rampino, M.R., Self, S., 1992. Volcanic winter and accelerated glaciation following the Toba super-eruption. Nature 359, 50–52.

Rampino, M.R., Stothers, R.B., 1984a. Terrestrial mass extinctions, cometary impacts and the Sun's motion perpendicular to the Galactic plane. Nature 308, 709–712.

Rampino, M.R., Stothers, R.B., 1984b. Geological rhythms and cometary impacts. Science 226, 1427–1431.

Rampino, M.R., Stothers, R.C., 1988. Flood basalt volcanism during the past 250 million years. Science 241, 663–668.

Rampino, M.R., Haggerty, B.M., Pagano, T.C., 1997. A unified theory of impact crises and mass extinctions: quantitative tests. Annals of the New York Academy of Sciences 822, 403–431.

Rampino, M.R., Prokoph, A., Adler, A.C., 2000. Tempo of the end-Permian event: high-resolution cyclostratigraphy at the Permian–Triassic boundary. Geology 28, 643–646.

Raup, D.M., Sepkoski Jr., J.J., 1986. Periodic extinction of families and genera. Science 231, 833–836.

Remane, J., 2003. Chronostratigraphic correlations: their importance for the definition of geochronologic units. Palaeogeography, Palaeoclimatology, Palaeoecology 196, 7–18.

Rioul, O., Vetterli, M., 1991. Wavelets and signal processing. The Institute of Electrical and Electronics Engineers Special Magazine, 14–38.

Sellwood, B.W., Price, G.D., Valdes, P.J., 1994. Cooler estimates of Cretaceous temperatures. Nature 370, 453–455.

Shackleton, N.J., Imbrie, J., 1990. The $\delta^{18}O$ spectrum of oceanic deep water over a five-decade band. Climate Change 16, 217–230.

Shackleton, N.J., Kennett, J.P., 1975. Paleotemperature history of the Cenozoic and initiation of Antarctic glaciation: oxygen and carbon isotope analysis in DSDP Sites 277, 279 and 281. In: Kennett, J.P., Houtz, R.E. (Eds.), Init. Rep. DSDP. US Gov. Print. Off, Washington, DC, pp. 743–755.

Smolukowski, R., Bahcall, J.N., Matthews, M. (Eds.), 1986. The Galaxy and the Solar System. Univ. of Arizona Press, Tucson.

Stothers, R.B., 1993a. Impact cratering at geologic stage boundaries. Geophysical Research Letters 20, 7–890.

Stothers, R.B., 1993b. Flood basalts and extinction events. Geophysical Research Letters 20, 1399–1402.

Torrence, C., Compo, G.P., 1998. A practical guide to wavelet analysis. Bulletin of American Meteorological Society 79, 61–78.

Veizer, J., Ala, D., Azmy, K., Bruckschen, P., Buhl, D., Bruhn, F., Carden, G.A.F., Diener, A., Ebneth, S., Goddéris, Y., Jasper, T., Korte, C., Pawellek, F., Podlaha, O.G., Strauss, H., 1999. $^{87}Sr/^{86}Sr$, ^{13}C and ^{18}O evolution of Phanerozoic seawater. Chemical Geology 161, 59–88.

Vogt, P.R., 1989. Volcanogenic upwelling of anoxic, nutrient-rich water: a possible factor in carbonate-bank/reef demise and benthic faunal extinctions? Geological Society of America Bulletin 101, 1225–1245.

Voigt, S., 2000. Stable oxygen and carbon isotopes from brachiopods of southern England and northwestern Germany: estimation of Upper Turonian palaeotemperatures. Geological Magazine 137, 687–703.

Zachos, J., Pagani, M., Sloan, L., Thomas, E., Billups, K., 2001. Trends, rhythms, and aberrations in global climate 65 Ma to present. Science 282, 686–693.